J Physiol 590.18 (2012) pp 4483–4499

The Journal of Physiology

An updated computational model of rabbit sinoatrial action potential to investigate the mechanisms of heart rate modulation

Stefano Severi[1], Matteo Fantini[1], Lara A. Charawi[2] and Dario DiFrancesco[3]

[1] *Biomedical Engineering Laboratory – D.E.I.S., University of Bologna, Via Venezia 52, 47521 Cesena, Italy*
[2] *Department of Mathematics, University of Milano, Via Saldini 50, 20133 Milano, Italy*
[3] *Department of Life Sciences, University of Milano, Via Celoria 26, 20133 Milano, Italy*

Key points

- Computational models of the electrical activity of sinoatrial cells (SANCs) have been proposed to gain a deeper understanding of the cellular basis of cardiac pacemaking.
- However, they fail to reproduce a number of experimental data, among which are effects measured after modifications of the 'funny' (I_f) current.
- We developed a novel SANC mathematical model by updating the description of membrane currents and intracellular mechanisms on the basis of experimental acquisitions, in an attempt to reproduce pacemaker activity and its physiological and pharmacological modulation.
- Our model describes satisfactorily experimental data on pacemaking regulation due to neural modulation, I_f block and inhibition of the intracellular Ca^{2+} handling.
- Computer simulation results suggest that a detailed description of the intracellular Ca^{2+} fluxes is fully compatible with the observation that I_f is a major component of pacemaking and heart rate modulation.

Abstract The cellular basis of cardiac pacemaking is still debated. Reliable computational models of the sinoatrial node (SAN) action potential (AP) may help gain a deeper understanding of the phenomenon. Recently, novel models incorporating detailed Ca^{2+}-handling dynamics have been proposed, but they fail to reproduce a number of experimental data, and more specifically effects of 'funny' (I_f) current modifications. We therefore developed a SAN AP model, based on available experimental data, in an attempt to reproduce physiological and pharmacological heart rate modulation. Cell compartmentalization and intracellular Ca^{2+}-handling mechanisms were formulated as in the Maltsev–Lakatta model, focusing on Ca^{2+}-cycling processes. Membrane current equations were revised on the basis of published experimental data. Modifications of the formulation of currents/pumps/exchangers to simulate I_f blockers, autonomic modulators and Ca^{2+}-dependent mechanisms (ivabradine, caesium, acetylcholine, isoprenaline, BAPTA) were derived from experimental data. The model generates AP waveforms typical of rabbit SAN cells, whose parameters fall within the experimental ranges: 352 ms cycle length, 80 mV AP amplitude, −58 mV maximum diastolic potential (MDP), 108 ms APD_{50}, and 7.1 V s^{-1} maximum upstroke velocity. Rate modulation by I_f-blocking drugs agrees with experimental findings: 20% and 22% caesium-induced (5 mM) and ivabradine-induced (3 μM) rate reductions, respectively, due to changes in diastolic depolarization (DD) slope, with no changes in either MDP or take-off potential (TOP). The model consistently reproduces the effects of autonomic modulation: 20% rate decrease with 10 nM acetylcholine and 28% increase with 1 μM isoprenaline, again entirely due

DOI: 10.1113/jphysiol.2012.229435

to increase in the DD slope, with no changes in either MDP or TOP. Model testing of BAPTA effects showed slowing of rate, −26%, without cessation of beating. Our up-to-date model describes satisfactorily experimental data concerning autonomic stimulation, funny-channel blockade and inhibition of the Ca^{2+}-related system by BAPTA, making it a useful tool for further investigation. Simulation results suggest that a detailed description of the intracellular Ca^{2+} fluxes is fully compatible with the observation that I_f is a major component of pacemaking and rate modulation.

(Received 31 January 2012; accepted after revision 15 June 2012; first published online 18 June 2012)
Corresponding author S. Severi: Biomedical Engineering Laboratory – D.E.I.S., University of Bologna, Via Venezia 52, 47521, Cesena (FC), Italy. Email: stefano.severi@unibo.it

Abbreviations AP, action potential; APA, action potential amplitude; APD, action potential duration; APD_{50}, action potential duration at its half-amplitude; CL, cycle length; DD, diastolic depolarization; HCN4, hyperpolarization-activated cyclic nucleotide-gated channel 4; HSMN, Himeno *et al.* (2008); ISO, isoprenaline; KO, knockout; KHIS, Kurata *et al.* (2002); LCR, local Ca^{2+} release; LDDC, linear diastolic depolarization component; MDD slope, mean DD slope; MDP, maximum diastolic potential; NDDC, non-linear diastolic depolarization component; POP, peak overshoot potential; SAN, sinoatrial node; SERCA, sarco-endoplasmic reticulum Ca^{2+}-ATPase; SR, sarcoplasmic reticulum; TOP, take-off potential.

Introduction

The cellular basis of the pacemaker activity of the sinoatrial node (SAN), and specifically the degree of contribution of the different mechanisms involved, is still debated (Lakatta & DiFrancesco, 2009; DiFrancesco, 2010; Lakatta *et al.* 2010; Noble *et al.* 2010; Verkerk & Wilders, 2010; Rosen *et al.* 2012; DiFrancesco & Noble, 2012; Maltsev & Lakatta, 2012).

Reliable mathematical models of the SAN action potential (AP) may help gain a deeper understanding of the phenomenon. Indeed, many models of SAN AP have been developed (see Wilders (2007) for a review) since the first mathematical models reproducing pacemaker activity were created (McAllister *et al.* 1975; DiFrancesco & Noble, 1982; Noble & Noble, 1984; DiFrancesco & Noble, 1985).

More recently, two novel SAN AP models incorporating detailed calcium-handling dynamics have been proposed. Himeno *et al.* (2008) updated the Sarai *et al.* (2003) model by incorporating the β_1-adrenergic signalling cascade in a guinea pig SAN model (referred throughout the paper as the HSMN model) in order to investigate the ionic mechanisms underlying the positive chronotropy. Maltsev & Lakatta (2009) proposed a rabbit SAN model (referred to throughout the paper as the ML model), mainly based on the Kurata model (Kurata *et al.* 2002) (referred to throughout the paper as the KHIS model) more specifically addressing the interactions between intracellular calcium handling and membrane currents. The HSMN and ML models have been also recently compared (Himeno *et al.* 2011) in order to analyse the extent to which cytosolic Ca^{2+} affects SAN pacemaker activity.

However, it is worth noting that despite the significant improvements introduced by such models in the description of SAN cell electrophysiology, neither the HSMN nor the ML model reproduces the experimental effects of 'funny' current (I_f) reduction. In fact, a large amount of data coming from different laboratories (Table 1) shows that the use of drugs at concentrations known to produce only partial block of I_f leads to significant AP rate decrease. On the contrary, simulation of complete block of I_f produces only minor rate reduction in the HSMN and ML models (about 1% and 5%, respectively). This limitation of present models seems particularly important when considering that most of the debate about the genesis of pacemaking is focused on the role of I_f current *versus* calcium oscillations (Lakatta & DiFrancesco, 2009) and significantly weakens the usefulness of numerical simulation in the investigation of the mechanisms of physiological and pharmacological pacemaking modulation.

Moreover, from simulation results an open question arises: is the lack of effects of I_f block in the current models a direct consequence of the improved description of calcium handling? If this is the case, the role of I_f would have been previously overestimated because of the lack of detailed knowledge on calcium handling. Or is the lack of sensitivity to I_f block a consequence of an inaccurate description of the membrane currents? In the latter case an improvement of their mathematical formulation is needed in order to profitably use the computational approach to help understand the subtle mechanisms underlying pacemaking modulation.

Our main aim was to develop a SAN AP model rigorously based on available experimental data, and to compare the predictions of numerical analysis with the experimental rate modulation induced by autonomic stimulation, by I_f blockers and by changes in the Ca^{2+} transients. More specifically, we tested the hypothesis that a

Table 1. Effects of I_f blockade

Blocker	Dose	Expected percentage block	AP rate decrease
Caesium	2 mM	<69% at −50 mV (DiFrancesco *et al.* 1986)	20.3 ± 3.6% (Nikmaram *et al.* 1997) 30% (Denyer & Brown, 1990) 5.2 ± 0.3% (Vinogradova *et al.* 2002)
	6 mM	∼69% at −50 mV (DiFrancesco *et al.* 1986)	23.9% (Choi *et al.* 1999)
Ivabradine	3 μM	78% at −70 mV 66% at −100 mV (Bucchi *et al.* 2002) 58% at −100 mV (Bois *et al.* 1996)	16.2 ± 1.5% (Bucchi *et al.* 2007) 23.8 ± 3.9% (Thollon *et al.* 1994)
	1 μM	42% at −100 mV (Bucchi *et al.* 2002) 32% at −100 mV (Bois *et al.* 1996)	12.3 ± 5.2% (Thollon *et al.* 1994)

AP rate reduction due to different levels of I_f block measured experimentally.

quantitatively important role of I_f in pacemaking and rate modulation is fully compatible with the recently proposed description of intracellular calcium handling. We selected the rabbit SAN as a basis for our model, and aimed at using species-specific data whenever possible for improved consistency. The model was constructed based on the mathematical formulation of rigorously selected ionic currents and pump/exchange mechanisms derived from relevant published experimental data, mostly obtained in voltage clamp experiments. The model was then validated by simulating the action of pharmacological and autonomic agents that modulate SAN rate and comparing numerical reconstructions with experimental results from the literature.

Methods

SAN AP model approach and development strategy

The specific aim of our study was to develop a new computational rabbit SAN AP model able to reproduce existing experimental data on pacemaker rate generation and modulation, with a specific focus on data concerning experimental effects of I_f modulation. The framework of the model and the computational strategy were the same as in previously published work (e.g. DiFrancesco & Noble, 1985).

The general approach was not to incorporate in the model new assumptions leading to modifications in the model structure, but rather to critically review the formulations of membrane currents, pumps and exchangers in light of experimental results requiring a more accurate description.

Figure 1 shows a schematic diagram of our model. Since the major new feature of the ML model was a more advanced and tuned formulation of the sarcoplasmic reticulum (SR) function, we kept all the intracellular Ca^{2+} handling (cell structure/compartmentalization, SR Ca^{2+} release and SR Ca^{2+} pump) unchanged with respect to the ML formulation. However, we only retained the membrane mechanisms for which clear experimental evidence is available for a quantitative relevant contribution to rabbit SAN activity. Moreover, several membrane currents/pumps/exchangers were reformulated based on a critical review of published rabbit experiments. Only minor parameter tuning was performed, as indicated in the subsections below, in order to improve the overall features of the simulated action potential.

The model was implemented following the classical Hodgkin–Huxley formulation. Details for each current are described below. All model equations and parameter values are provided as Supplemental Material.

Identification of simulated currents

Funny current (I_f). I_f is described as composed of two relatively independent Na^+ and K^+ components, I_{fNa} and I_{fK}, whose contributions to the total conductance at normal Na^+ and K^+ concentrations are similar, as

according to the original description (DiFrancesco & Noble, 1982), I_f is also modulated by the extracellular potassium concentration K_o. We assumed as in the DiFrancesco–Noble model (DiFrancesco & Noble, 1985) that this dependence is a first order binding process. At the concentration of 5.4 mM, the maximal conductances $g_{f,Na}$ and $g_{f,K}$ have the same value of about 3.2 nS.

For the gating mechanism, we adopted Hodgkin–Huxley second order kinetics as in Noble *et al.* (1989). More recent models also adopted a similar description (Wilders *et al.* (1991); KHIS; ML). Our formulation of the steady-state activation curve fits the experimental results of Altomare *et al.* (2003) and Barbuti *et al.* (2007) and describes an activation curve positioned around a half-activation potential of −64 mV; notice that the previous KHIS and ML SAN models, based on data from Van Ginneken & Giles (1991), assumed a much more negative activation curve (Fig. 2*A*).

The time constant curve (τ_f) was formulated on the basis of data from Noble *et al.* (1989) (Fig. 2*B*). Here too, our τ_f curve is shifted to more depolarized voltages relative to that of other models.

L-type calcium current (I_{CaL}). The kinetics of $I_{Ca,L}$ are described by voltage-dependent activation (d_L), voltage-dependent inactivation (f_L), and Ca^{2+}-dependent inactivation (f_{Ca}) gating variables.

The voltage dependences of the steady-state activation and inactivation curves ($d_{L\infty}$ and $f_{L\infty}$) are shown in Fig. 3. Their formulations were based on data from Fermini & Nathan (1991).

Previous models (Demir *et al.* (1994); KHIS; ML) quoted the same experimental data as the basis for their description of $I_{Ca,L}$, though with additional adjustments, included to improve the fitting of action potential data, that make their activation curve formulation significantly different from experimental results (Fig. 3).

Expression of the activation time constant d_L was based, as already done for the above models, on the whole cell data of Nilius (1986) (guinea pig SAN myocytes at 25°C), because specific data on rabbit SAN are not available. According to Demir *et al.* (1994), a Q_{10} factor of 2.3 was applied to scale these data up to a temperature of 37°C. We formulated the inactivation time constant from the data of Nakayama *et al.* (1984), Hagiwara *et al.* (1988) and Kawano & Hiraoka (1991).

Formulas for the Ca^{2+}-dependent inactivation f_{Ca} were adopted from the KHIS model, as in the ML model.

We adopted the constant-field formulation to describe the conductance property of $I_{Ca,L}$, which is also known to have small but not negligible components carried

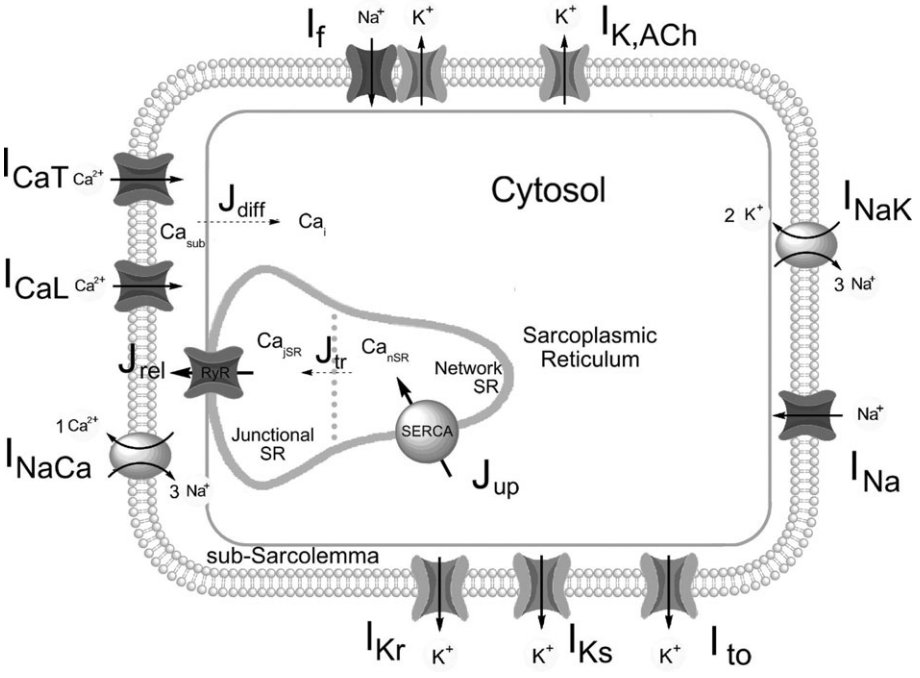

Figure 1. Diagram of the model
Schematic diagram of the model depicting cell compartments and major functional components. Fluid compartments include cytosol, subsarcolemmal space and sarcoplasmic reticulum (network and junctional SR). Membrane currents are shown with associated ion selectivities (see Supplemental Material for abbreviations). The Ca^{2+}-handling system comprises Ca^{2+} diffusion from submembrane space to myoplasm (J_{diff}), Ca^{2+} uptake by SR (J_{up}), Ca^{2+} pump (SERCA), transfer between network and junctional SR (J_{tr}), and release (J_{rel}) by ryanodine receptors (RyRs).

by Na^+ and K^+ ions. The relative permeabilities of these components were set as in the model by Sarai *et al.* (2003). The calcium permeability was set to 0.2 nA mM^{-1} to provide a $I_{Ca,L}$ density of 7 pA pF^{-1}, within the experimental range (7.7 ± 2.3 pA pF^{-1}) reported by Honjo *et al.* (1996) in rabbit SAN cells.

T-type calcium current ($I_{Ca,T}$). As in the case with $I_{Ca,L}$, the steady state activation and inactivation curves (Fig. 4*A*), $d_{t\infty}$ and $f_{t\infty}$ respectively, are the Boltzmann curves fitting the data of Fermini & Nathan (1991). The ML, KHIS and Demir *et al.* (1994) models also referred to data from Hagiwara *et al.* (1988).

The expression for the time constant of inactivation was obtained by fitting data from the study of Hagiwara *et al.* (1988), through a least square procedure. As done with $I_{Ca,L}$, to describe the $I_{Ca,T}$ conductance we opted for the constant-field equation, setting the Ca^{2+} permeability to 0.02 nA mM^{-1}, which allowed to maintain a stable total current during diastolic depolarization (DD).

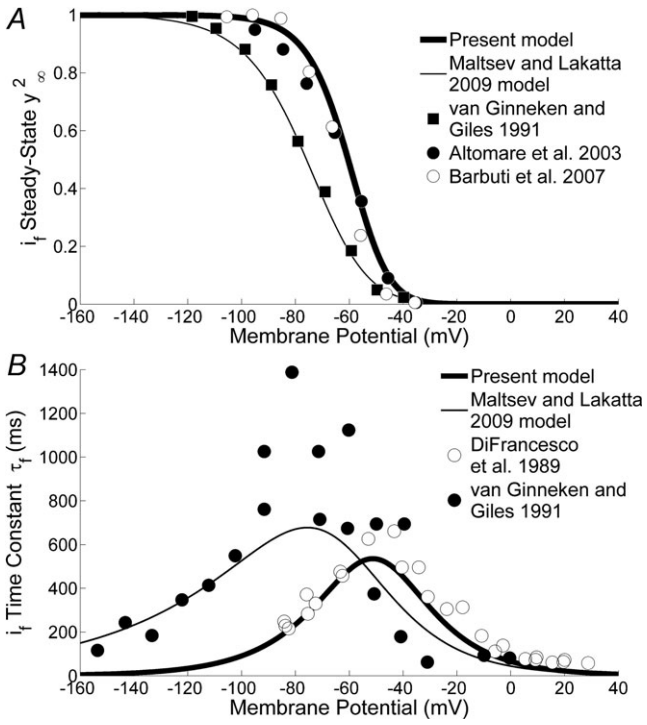

Figure 2. Funny current
A, I_f activation curve. Plotted are the curve used in our model (thick line), based on data from Altomare *et al.* (2003) and Barbuti *et al.* (2007) (filled and open circles, respectively) and the curve used in the ML model (thin line), based on data from van Ginneken & Giles (1991) (filled squares). Fitting is performed using the second power of the gating variable *y*, as formulated in the two models. *B*, I_f time constant curve. Comparison between our curve (thick line) based on the square kinetics assumption of Noble *et al.*'s (1989) experimental data (open circles) and the ML model curve (thin line) based on van Ginneken & Giles (1991) data (filled circles).

Rapid and slow delayed rectifier K^+ currents (I_{Kr}, I_{Ks}). Extensive studies have shown that the total delayed rectifier potassium current can be separated into a rapidly activating I_{Kr} and a slowly activating I_{Ks} component (Sanguinetti & Jurkiewicz, 1990). The expression of these components in SAN cells are species dependent; in rabbit SAN, both currents are present, but I_{Kr} is the predominant component. Although the contribution of I_{Ks} to beating rate is small under control conditions, it becomes significant during β-adrenergic stimulation (Lei *et al.* 2002).

To describe the gating mechanism of I_{Kr}, previous models (such as Demir *et al.* (1994) and Dokos *et al.* (1996)) used equations provided by Shibasaki (1987) for rabbit node cells. Later models such as ML and its parent model KHIS based the formulation of the kinetics of I_{Kr} on the work of Ono & Ito (1995) on rabbit SAN cells at ~33°C, reporting a complete set of quantitative data on current activation. According to their study, activation and deactivation of I_{Kr} are well modelled by two activation variables: a fast activation variable (p_{af}) and a slow one (p_{as}). The general activation variable (p_a) is a convex linear combination of p_{af} and p_{as}.

We based the mathematical description of the activation and inactivation kinetics of I_{Kr} mainly on that of Ono & Ito

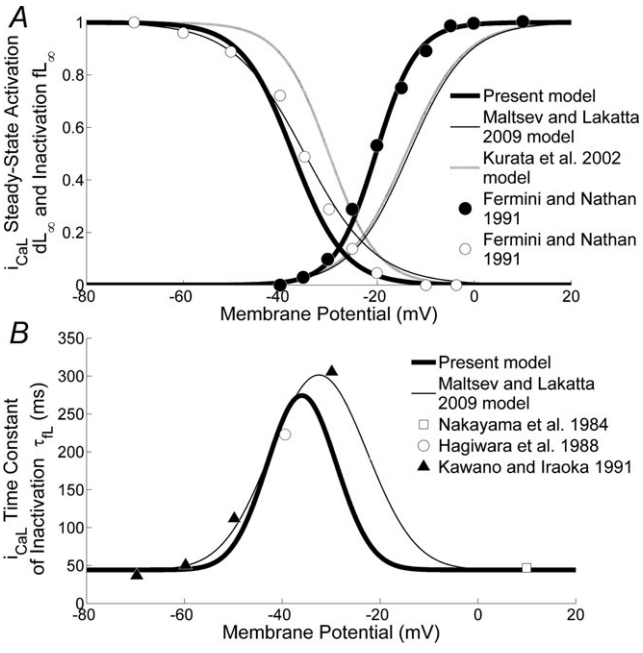

Figure 3. I_{CaL} current
A, $I_{Ca,L}$ activation and deactivation curves. Our activation and deactivation curves (thick lines), based on Fermini & Nathan's (1991) data (filled and open circles, respectively), are compared with those of the KHIS (grey line) and ML models (thin line). *B*, time constant of $I_{Ca,L}$ inactivation. The plot shows our curve (thick line), the curve of the ML model (thin line) and experimental data from Nakayama *et al.* (1984) (open squares), Hagiwara *et al.* 1988 (open circles) and Kawano & Hiraoka (1991) (filled triangles).

(1995). In order to improve the overall AP morphology, the time constant of fast activation τ_{af} was slightly modified, while the steady state activation variable ($p_{a\infty}$) was based on data by Lei & Brown (1996), from rabbit SAN cells at 37°C. Activation and inactivation curves and activation time constant curves are shown in Fig. 5. Since no detailed experimental data were reported by Ono & Ito (1995) on the voltage dependence of the time constant of inactivation, for this variable we used the expression provided by Shibasaki (1987), as in the ML model.

We described the slow activation of I_{Ks} (gate n) according to the formulation of Zhang *et al.* (2000), previously adopted also by the KHIS and ML models, in which current kinetics are modelled using second order Hodgkin–Huxley equations. The expression of the steady-state variable was from data in Lei & Brown (1996).

There are limited experimental data for the voltage dependence of the I_{Ks} time constant, τ_n, in rabbit SAN cells. The Zhang *et al.* (2000) model used a formulation from Heath & Terrar (1996), based on their data from guinea-pig ventricular cells. We modified the formulation of the time constant curve (Fig. S1*A* Supplemental Material) and set the conductance g_{Ks} to 1.7 nS in order to reproduce the AP-clamp results from rabbit SAN cells of Lei *et al.* (2002) (Fig. S1*B* and *C*, Supplemental Material).

Sodium-potassium pump (I_{NaK}). I_{NaK} was described as according to the original description in KHIS, based on experimental data of Sakai *et al.* (1996) from rabbit SAN cells at 37°C. In models preceding the KHIS model, the expression of I_{NaK} was not based on data from SAN cells (KHIS). The voltage-dependent factor in the equation controlling the pump activity at diastolic voltages was steeper in our formulation than in the ML formulation (Fig. S2, Supplemental Material); we verified that this voltage dependence is associated with a range of calculated MDP values closer to values experimentally measured (Table 2).

Transient outward (I_{to}) K^+ current. We adopted the same set of equations as in the ML model, as modified from KHIS.

Acetylcholine-dependent ($I_{K,ACh}$) K^+ current. The starting formulation for the $I_{K,ACh}$ current was provided by the HSMN model, in turn derived from the Sarai *et al.* (2003) model, where the gating variables of $I_{K,ACh}$ (α_a and β_a) both depend upon membrane potential and ACh concentration.

The work by DiFrancesco *et al.* (1989) in rabbit SAN cells at 35–36°C includes measurement of $I_{K,ACh}$ at the

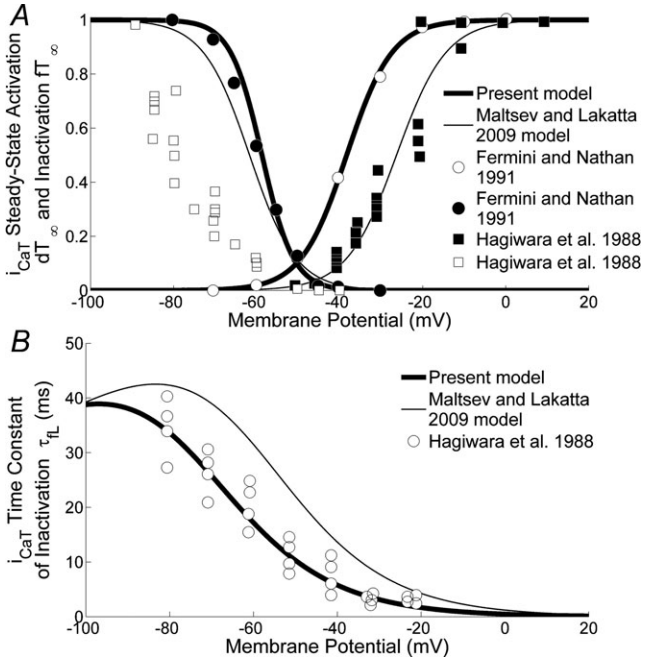

Figure 4. I_{CaT} current
A, $I_{Ca,T}$ activation and deactivation curves. Our activation and deactivation curves (thick lines), based on Fermini & Nathan's (1991) data (filled and open circles, respectively), are plotted along with the curves of the ML model (thin lines) and Hagiwara *et al.*'s (1988) data (filled and open squares, respectively). *B*, time constant of $I_{Ca,T}$ inactivation. Compared are our curve (thick line), based on Hagiwara *et al.* (1988) (open circles) and the ML model curve (thin line).

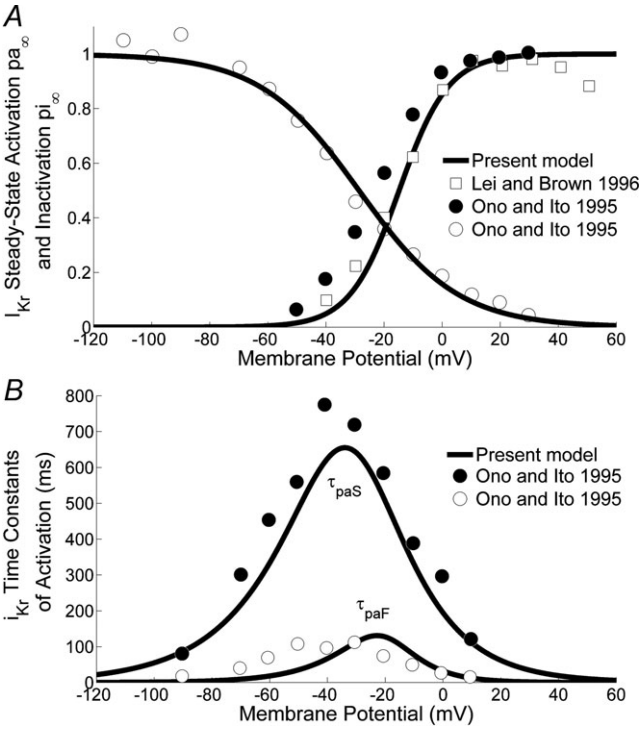

Figure 5. I_{Kr} current
A, I_{Kr} activation and deactivation curves together with Ono & Ito's (1995) (open and filled circles) and Lei & Brown's (1996) (open squares) data. *B*, time constant for fast and slow I_{Kr} activation and Ono & Ito's (1995) data.

Table 2. Comparison of characteristics of simulated and experimental APs

Characteristics	KHIS model (Kurata *et al.* 2002)	ML model (Maltsev & Lakatta, 2009)	Present model	Experimental values (mean ± SD (range))
CL (ms)	380	333	352	325 ± 42(247 ÷ 389)
MDP (mV)	−59	−63	−58	−56 ± 6(−66 ÷ −52)
APA (mV)	79	76	80	87 ± 6(78 ÷ 98)
POP (mV)	20	16	22	27 ± 5(20 ÷ 32)
APD_{50} (ms)	120	101	108	93 ± 12(73 ÷ 111)
dV/dt_{max} (V s^{-1})	7.6	4.8	7.1	11.3 ± 6.5(4.8 ÷ 27)

Simulation data from different models compared with experimental AP characteristics from 12 studies at physiological temperatures (Table 1 in Kurata *et al.* (2002)). CL, cycle length; MDP, maximum diastolic potential; APA, action potential amplitude; POP, peak overshoot potential; APD_{50}, AP duration at its half-amplitude; dV/dt_{max}, maximum rate of rise of membrane potential during AP upstroke.

holding potential of −40 mV in the presence of different ACh concentrations. By fitting these experimental data we obtained an updated formulation for the ACh-dependence of the gating variable.

Sodium current (I_{Na}). In SAN cells, I_{Na} is a very small current. For its formulation we used the equations from Noble *et al.* (1989).

Sodium-calcium exchanger (I_{NaCa}) and sarcoplasmic reticulum (SR) currents. We used the same set of equations as in the ML and KHIS models.

Ion concentrations. The mass balance equations were used to describe the Ca^{2+} dynamics in the intracellular compartments. Even though the internal Na^+ compartmentation is still incompletely understood, we also included the temporal variations in intracellular Na^+ concentration.

Cell capacitance and dimensions. We used the same parameters as in the ML model.

Hardware and software

For simulations we used Cellular Open Resource (COR) (Garny *et al.* 2009) on a Windows 7 PC with an Intel Core 2 Quad processor. Integration was performed by CVODE algorithm, using Backward Differentiation Formula (BDF) together with a Newton iteration. All simulations were run until steady state (assessed by observation of intracellular sodium concentration) unless otherwise noted.

Model code can be requested from the authors and will be published in the CellML repository.

Identification of individual model components (i.e. steady state curves, time constants, etc.) was performed by custom code written in Matlab 2009a (The Mathworks, Inc., Natick, MA, USA), with a least squares approach, or through manual parameter estimation, where minimization was by simple guess and check.

Results

Features of simulated rabbit san cell action potential

AP waveforms generated by the model (Fig. 6*A*) mimic closely those recorded in rabbit SAN cells in normal Tyrode solution at a temperature of 34–37°C. The main AP parameters measured in the standard model configuration are reported in Table 2. All values fall within published experimental ranges and are similar to those of previous SAN AP models (see for example the KHIS and ML models in Table 2).

In order to quantitatively describe the specific properties of DD, we tested the model with the method proposed and applied by Bogdanov *et al.* (2006) to characterize the different DD components in rabbit SAN AP. The DD is divided in two phases: the linear DD component (LDCC) and the non-linear one (NDDC). As reported in Table 3, our model correctly reproduces the subdivision of DD in the two phases, with a LDDC duration (NDCC delay in Table 3, according to Bogdanov *et al.* (2006)) lasting 78% of the total DD duration. However, a steeper mean slope of the linear component (MDD slope) was measured in the simulated APs. Notably Bucchi *et al.* (2007) found a basal value for MDD slope (called EDD in their paper) of 101 mV ms^{-1} at 2.9 Hz, which is very similar to the values of our model (101 mV ms^{-1} at 2.8 Hz).

The validity of the model was further assessed by reconstructing a classical voltage clamp experiment by which activation of I_f is elicited on hyperpolarization and both I_K and I_{CaL} are activated upon depolarization. As shown in Fig. S4, model voltage clamp results agree with typical experimental results.

In Fig. 6*B*–*F* and *H*–*I* the time course of ionic currents and intracellular ion concentrations under AP (Fig. 6*A*)

Table 3. Comparison of simulated and experimental features of diastolic depolarization (DD)

Characteristics	KHIS model (Kurata *et al.* 2002)	ML model (Maltsev & Lakatta, 2009)	Present model	Experimental values (Bogdanov *et al.* 2006)
TOP (mV)	−40	−39	−41	−46 ± 1
DD duration (ms) (percentage of CL)	123 (32%)	168 (50%)	185 (52%)	194 ± 9(56%)
MDD slope (mV s^{-1})	168	153	101	57 ± 4
NDDC amplitude (mV)	18	18	21	20 ± 1
NDDCτ (ms)	15	23	13	17 ± 1
NDDC delay (ms) (percentage of DD duration)	78 (63%)	99 (59%)	145 (78%)	145 ± 8(75%)

TOP, take-off potential; MDD slope, mean DD slope measured during the first two-thirds of the DD; NDDC, non-linear DD component; NDDCτ, time constant of exponential fitting of non-linear component; NDDC delay, time interval between time when MDP is reached and when NDDC reaches 5% of its amplitude.

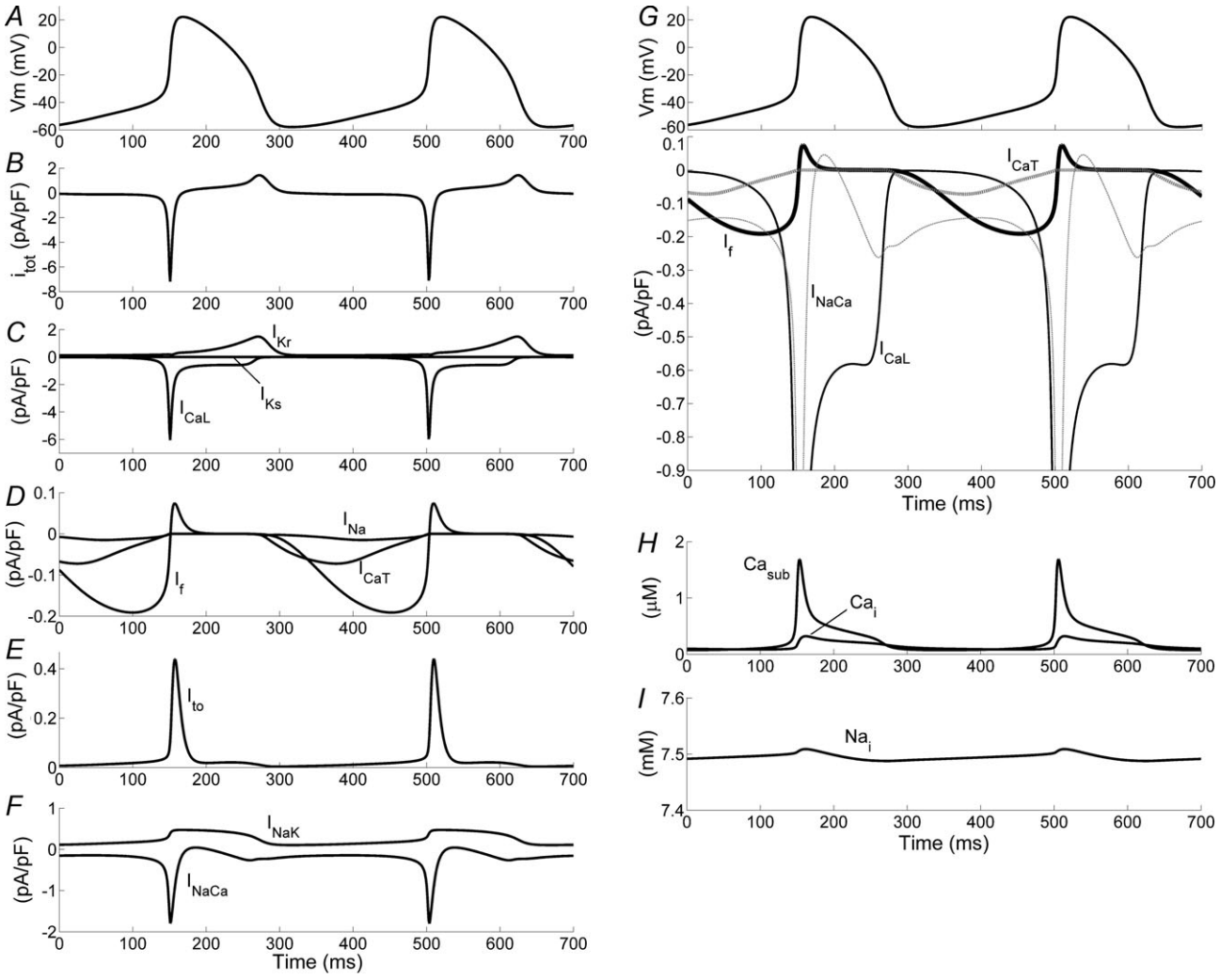

Figure 6. Simulation of 700 ms of spontaneous electrical activity in the rabbit SA node
A–F, action potential, total ionic current and individual currents, pump and exchanger components are plotted as indicated. *G*, superimposition of inward membrane currents relevant to DD. *H* and *I*, Ca^{2+} transients and intracellular Na^{+} concentration.

are plotted. Inward components during DD are also plotted together in Fig. 6*G* to highlight their relative contributions. It can be seen that I_f slowly increases during DD, reaching its maximum in the second half of DD, whereas I_{NaCa} has a biphasic time course, decreasing in the first half of DD and then increasing (thus contributing to depolarization) in the second half. The contribution of $I_{Ca,T}$ is minor, whereas $I_{Ca,L}$ increases rapidly at the end of DD thus promoting the AP upstroke.

Effects of I_f blockade

The action of ivabradine was simulated by a partial block of funny channels (66% reduction of I_f conductance, as reported with a 3 μM concentration by Bucchi *et al.* (2002), Table 1). The assumption of a constant block during pacemaking activity was considered to be a good approximation because of the extremely slow block kinetics of ivabradine (Bucchi *et al.* 2002). During an activation/deactivation protocol (or during action potentials), ivabradine block develops very slowly, and attains eventually a steady-state level that can be assumed to remain constant during the protocol itself (or during activity), essentially independently of the kinetics of channel opening/closing.

The model predicts a reduction of spontaneous rate (Fig. 7*B*) of 22% in agreement with experimental findings (Table 1). The model also predicts a reduction of the LDDC slope from 101 to 72 mV s^{-1} (−29%) in accordance with the reported experimental value of −31.9 ± 4.5% (Bucchi *et al.* 2007). At the same time, neither the TOP (−42 *vs.* −41 mV) nor the MDP (−59 *vs.* −58 mV) is altered by the drug, as also verified experimentally (Bucchi *et al.* 2007). The overall time course of AP after ivabradine application is very similar to the experimental one (e.g. compare Fig. 7*B* and *D*). On the other hand, simulation of ivabradine effects, with the same percentage of I_f block, in the ML model leads to negligible effects (Fig. 7*E*).

The action of caesium was simulated by the voltage-dependent partial block of funny channels (Fig. 7*C*), as reported from experimental analysis with a 5 mM concentration (DiFrancesco *et al.* 1986).

The model predicts a reduction of spontaneous rate (Fig. 7*A*) of 20%, which agrees well with experimental findings with 2–6 mM of caesium (Table 1). The model also predicts a reduction of the LDDC slope from 101 to 68 mV s^{-1} (−33%) in agreement with the reported experimental value of −26% (Nikmaram *et al.* 1997). Also in this case, the TOP (−44 *vs.* −41 mV) and the MDP (−59 *vs.* −58 mV) are not significantly affected.

Since a concurrent modulation of K^+ channels by 5 mM Cs^+ cannot be excluded, the implementation of the voltage-dependent block of K^+ currents, as reported in Quayle *et al.* (1988), was also tested. The reduction in K^+ currents led to a slight depolarization of the MDP but did not affect the overall rate reduction obtained by acting on I_f only (data not shown). For simplicity we decided not to include the action of Cs^+ on K^+ currents in our model.

Autonomic modulation of rate

Acetylcholine (ACh)- and isoprenaline (Iso)-induced variations in beating rate were reproduced by the model in a way that is quantitatively consistent with experimental data.

The action of ACh (Fig. S3) was simulated by block of the $I_{Ca,L}$ current and SR Ca^{2+} uptake as in Maltsev & Lakatta (2010), by shifting the I_f activation curve with the relation used by Zaza *et al.* (1996) and based on the fitting of several sets of experimental data (DiFrancesco & Tromba, 1988; Dokos *et al.* 1996; Renaudon *et al.* 1997), and by activating $I_{K,Ach}$ according to data from DiFrancesco *et al.* (1989) (see also Supplemental Material).

The model predicts a reduction of spontaneous rate (Fig. 8*A*) of 19.6%, for 10 nM ACh, similar to the reported experimental value of 20.8 ± 3.2% (Bucchi *et al.* 2007). The model also predicts a reduction of the LDDC slope from 101 to 76 mV s^{-1} (−25%) to be compared with the reported experimental value of −29.3 ± 4.4% (Bucchi *et al.* 2007). At the same time, neither the TOP (−40 *vs.* −41 mV) nor the MDP (−59 *vs.* −58 mV) is altered by the drug, as verified experimentally (Bucchi *et al.* 2007).

In order to gain additional mechanistic insight, we determined the contribution of individual ion currents to the ACh-dependent rate decrease (i.e. by specifically applying the phenomenological ACh effect on each current individually). The results show that changes in I_f are dominant. Indeed I_f modification alone leads to a 13% rate decrease whereas a minor effect is obtained when simulating exposure of only J_{up} to ACh concentration (1.1% rate decrease); further modulation of $I_{Ca,L}$ and $I_{K,Ach}$ does not affect at all the pacemaking rate. Similar results were obtained by simulating ACh effects on all targets but one: when I_f was the only unchanged current, the rate reduction was only 1.4%, suggesting that I_f alone contributes more than 18%. In the same way, the residual contributions of $I_{K,Ach}$ and J_{up} were calculated as 5.2% and 2.8%, respectively. No contribution of $I_{Ca,L}$ to rate reduction was seen.

Isoprenaline-induced rate acceleration, especially at low-to-moderate doses, is attributable mostly to the shortening of DD associated with a faster slope of DD, while action potential duration and shape vary minimally (Bucchi *et al.* 2007; DiFrancesco, 2010). The positive chronotropic effects of Iso 1 μM (Fig. 8*C*) were simulated by shifting the I_f activation gating variables by 7.5 mV to more positive voltages (Zaza *et al.* 1996) and by modulating $I_{Ca,L}$, I_{Ks}, I_{NaK} and the Ca^{2+} release uptake rate

P_{up}. Specifically, 1 μM Iso increases the amplitude of $I_{Ca,L}$ by 75% (Vinogradova *et al.* 2002); this enhancement was reconstructed by shifting the activation curves (Nagykaldi *et al.* 1999; Ke *et al.* 2007) to more negative values (−8 mV), by decreasing the inverse of slope factor of the activation variable $d_{L\infty}$ (−31%) (Antoons *et al.* 2007), and by increasing the maximal conductance (+23%). Similarly, I_{Ks} maximal conductance was increased by 20% and its activation curves were shifted by 14 mV to more negative potentials in order to increase the current amplitude (Severi *et al.* 2009; Wilders *et al.* 2010). A 20% increase of the maximal conductance of I_{NaK} was also introduced, according to Zeng & Rudy (1995). Finally, since the presence of a β-adrenergic agonist affects the SR Ca^{2+} pump (Vinogradova *et al.* 2006), but no quantitative data are available, following the same approach as in Maltsev & Lakatta (2010), we estimated an increase of P_{up} of 25% of its control value.

The overall simulated effect of 1 μM Iso was a 28.2% rate increase, in good agreement with the reported experimental value of 26.3 ± 5.4% for the same Iso concentration (Bucchi *et al.* 2007). The rate increase was entirely due to increase in the DD slope, with only minor changes in MDP and TOP (Fig. 8*C*).

The assessement of the contribution of each individual ion current to the Iso-dependent rate increase showed that changes in I_f are dominant, but the other contributions are not negligible. Indeed, when simulating exposure of only one of the Iso targets, the following rate changes were obtained: I_f +26.7%, I_{Ks} +3.8%, J_{up} +4.5%, I_{NaK} −2.9%, $I_{Ca,L}$ +0.1%. Based on the simulation of Iso affecting all the targets but one the following residual contribution were obtained: I_f +17.2%, I_{Ks} +11.8%, J_{up} +1.1%, I_{NaK} −2.7%, $I_{Ca,L}$ +1.2%.

Simulation of rapid cytosolic and sub-sarcolemmal Ca^{2+} chelation by acute BAPTA application

Ca^{2+} buffering by BAPTA was simulated according to the KHIS model in both the cytoplasm and subsarcolemmal space (see Supplemental Material), in an attempt to reproduce Himeno *et al.*'s (2011) experiments. Model testing of BAPTA effects showed slowing of rate without cessation of beating (Fig. 9*A*) as reported by Himeno *et al.* (2011) in guinea pig SAN cells (Fig. 9*B*); this result could not be reproduced by the ML model (Fig. 9*C*). In our

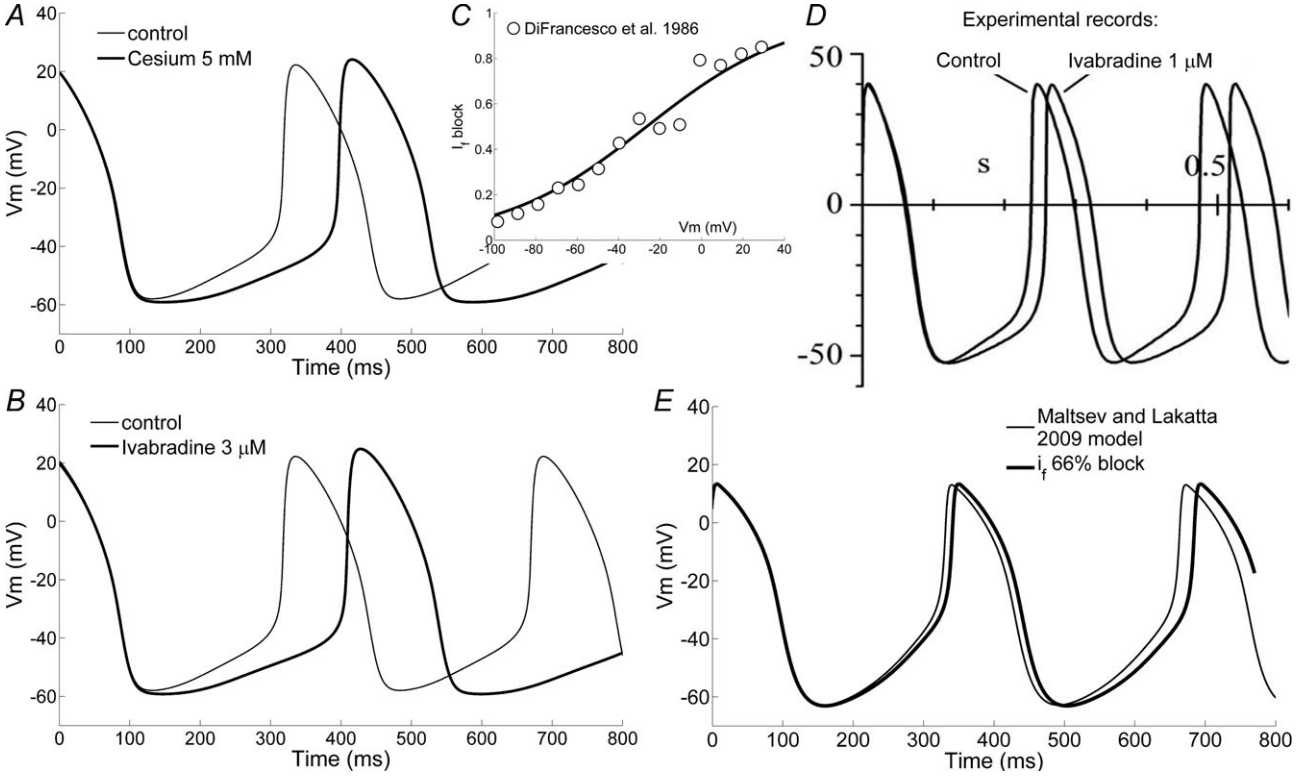

Figure 7. Effects of ivabradine and caesium on pacing
A and *B*, simulation of the action of 5 mM caesium and 3 μM ivabradine according to our SAN cell model. *C*, voltage dependence of I_f block by 5 mM Cs^+ used in our model to simulate the action of Cs^+, as based on DiFrancesco *et al.*'s (1986) data (open circles). *D*, experimental result with 1 μM ivabradine from DiFrancesco (2010). *E*, simulated effect of 66% block of I_f current in the ML model.

simulation the spontaneous CL was increased up to 443 ms (−26% rate) and the AP amplitude was also significantly decreased.

Model-based analysis of the effects on AP of I_f and Ca^{2+} handling modulation

The effects of I_f block is shown in Fig. 10*A*. Increasing levels of current block lead to progressive prolongation of the CL, up to complete cessation of pacemaking only when I_f is fully blocked.

Full removal of I_{NaCa} also leads to cessation of pacemaking (Fig. 10*C*, upper panel) but the effect of partial current block is completely different from that due to I_f blockade. In this case almost no modulation of the CL occurs upon block of up to 75% of the maximal I_{NaCa} current. The lack of effects on CL is due to a physiological compensatory effect: the decrease of I_{NaCa} tends to cause Ca^{2+} accumulation in the subsarcolemmal space, which in turn increases the outward I_{NaCa} current. As a result, even in the presence of a massive reduction of the maximal I_{NaCa} current, the size of the actual I_{NaCa} current flowing during DD remains almost constant (Fig. 10*C*, lower panel). Partial I_{NaCa} block also leads to only minor alterations in intracellular Na^+: from 7.5 to 7.35 mM and to 6.9 mM with a 75% and 90% blockade, respectively.

Modulation of Ca^{2+} handling processes through modification of the maximal SERCA pump current can also modulate pacemaking rate (Fig. 10*B*). Grading P_{up} from 1 to 40 mM s^{-1} increases the AP firing rate from 2.7 to 3.9 Hz. Notably, changes in CL are accompanied by changes in the morphology of DD, which becomes less linear (see Fig. 10*B*).

The presence in the model of the 'isolated Ca^{2+} oscillator' was tested by reproducing the simulations in which all membrane currents are set to 0 (see Fig. S5). As expected, the results are similar to those of Fig. 5*C* of Maltsev & Lakatta (2009). Moreover, we investigated the capability of the model to generate damped Ca^{2+} oscillations within the cell when the membrane potential is clamped at its maximum diastolic value (Fig. 11). Whereas an almost negligible oscillation in Ca^{2+} concentration is present in control conditions ($P_{up} = 12$ mM s^{-1}), oscillations are clearly seen when P_{up} is increased up to 40 mM s^{-1} (Fig. 11*B*). Notably, at this high value of the SERCA pump activity, the morphology of membrane potential is altered and there is no linear phase of DD (Fig. 11*A*).

The contribution of the different pathways to pacemaking was further investigated by performing a

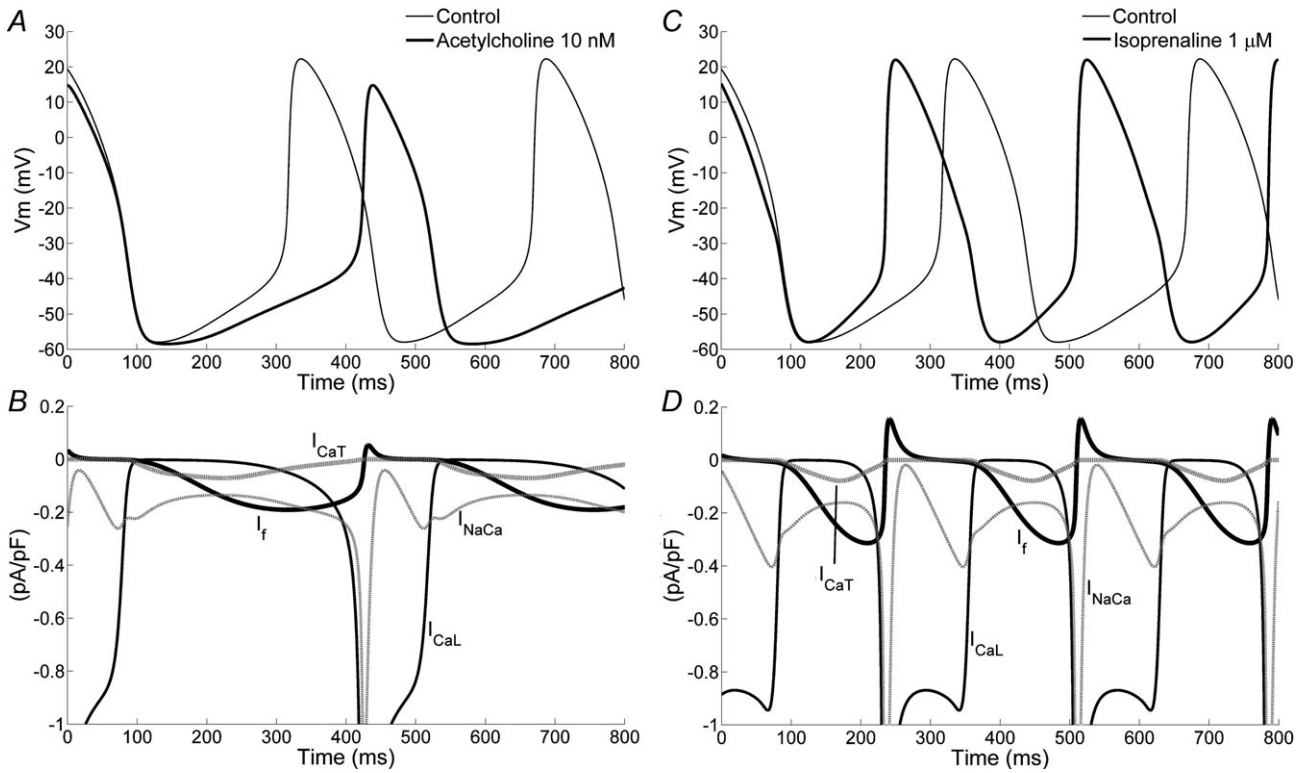

Figure 8. Action of acetylcholine and isoprenaline
A and *C*, simulation of the action of 10 nM ACh and 1 μM Iso on spontaneous activity. *B* and *D*, contribution of individual ion currents to the ACh- and Iso-dependent rate modulation, respectively.

model-based analysis in which the contributions of single membrane currents and subsarcolemmal Ca^{2+} concentration are dissected (Fig. 12). I_f block leads to stop of pacemaking if performed at either the time of MDP or at the beginning of the non-linear phase of DD. Clamping the Ca^{2+} concentration at the MDP value does not affect the early diastole but prolongs the late phase, without stopping pacemaking. When only the Ca^{2+} concentration 'sensed' by I_{NaCa} is clamped, such effects are enhanced, which is due to a lack of compensatory increase in I_{CaL} driving force when Ca^{2+} concentration is low.

To test if the contribution of I_f to pacemaking results directly from the specific choice of I_f formulation (see Fig. 1), we performed additional simulations. When the present model was run with a formulation of I_f kinetics based on van Ginneken & Giles's (1991) data, in basal conditions the CL was 386 ms (*vs.* 352 ms of the present model); thus, the decrease in I_f, as expected, leads to slowing of rate. When the action of 3 μM ivabradine was simulated we obtained a CL of 532 ms, that is rate was decreased by −27% (−22% in the present model).

When the present model was run with a formulation of I_f kinetics based on van Ginneken & Giles (1991) and the maximal conductance used in the ML model (that is, with the maximal conductance reduced by a factor of 2.375 with respect to van Ginneken & Giles's (1991) data), in basal conditions the CL was 505 ms. Simulation of the action of ivabradine led to 762 ms CL. Therefore, a strong sensitivity to I_f block was indicated by our model also when incorporating the I_f formulation used in previous models in which such sensitivity was not reproduced.

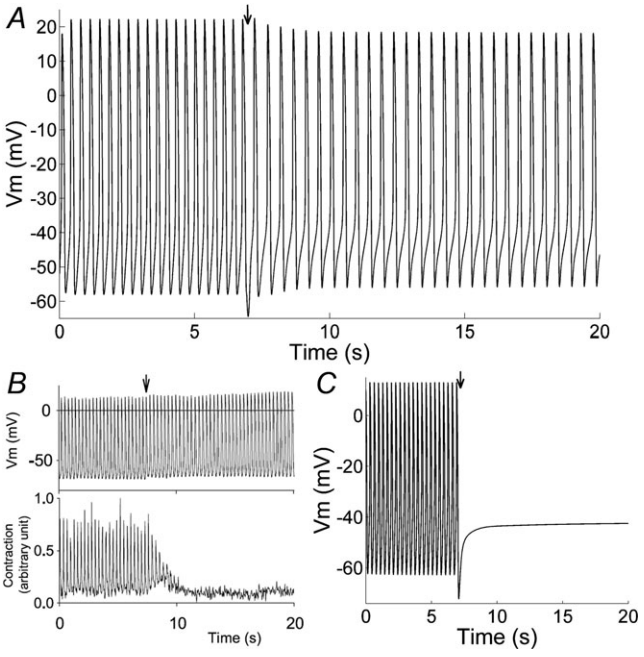

Figure 9. Action internal BAPTA
A, simulation of the effects of 10 mM BAPTA internal perfusion. *B*, spontaneous AP activity and cell contractions recorded experimentally upon perfusion with 10 mM BAPTA in guinea pig SAN cell (from Himeno *et al.* 2011, with permission of the American Physiological Society). *C*, same simulation in the ML model. Arrows in *A* and *C* indicate the beginning of the perfusion.

Discussion

We developed a novel computational model of physiological cardiac cell pacemaker function with the aim of reproducing a set of recent and less recent experimental data relevant to generation and control of pacemaker activity, and more specifically the changes of pacemaking function associated with changes in I_f current and Ca^{2+} handling as experimentally observed.

Our model describes satisfactorily the electrical activity of rabbit SAN cells and reproduces quantitatively experimental data on the action of autonomic rate modulation, f-channel blockade and inhibition of the Ca^{2+} transients by BAPTA, and can thus provide a basis for a more extended investigation.

A main assumption of this model, based on a wealth of experimental data (DiFrancesco, 2010), is that I_f is the major inward ionic current until late DD. This assumption differs substantially from those of previous recent SAN models such as the HSMN and ML models. Simulation results indicate that the above assumption of I_f being the major inward diastolic ionic current can be successfully integrated with a detailed description of the intracellular Ca^{2+} fluxes such as the one treated in the ML model, and is at the same time able to reproduce previously unexplained experimental results involving the modulation of both I_f and Ca^{2+} cycling.

A correct evaluation of the I_f activation curve is crucial to define the extent of the I_f contribution to pacemaking depolarization. Some discrepancies between different experimental data have long been reported and discussed (see e.g. DiFrancesco 1993). Current run-down, incomplete series resistance compensation, incomplete current activation at depolarized voltages, together with natural cell heterogeneity may have contributed to the underestimation of the size of I_f in previous reports. In building our model we decided to base the I_f formulation on data from rabbit SAN cells obtained in our laboratory, from experiments in which we were confident that all the possible confounding/altering factors had been carefully controlled.

Before validating our model against specific rate modulating agents, we assessed the basic AP characteristics. We compared the simulated AP features with the same set of experimental data used for validation of the KHIS and ML rabbit SAN models. As shown in Table 2, each of the basic characteristics of our model is within the range of experimental measurements.

One aspect of membrane potential morphology that is particularly relevant for SAN function is the profile of the slow diastolic depolarization (DD). It is well known that a distinctive feature of rabbit SAN AP is the linear increase of membrane potential during the early DD phase, followed by an exponential-like increase in the late DD phase. The latter is mainly driven by Ca^{2+} fluxes due to $I_{Ca,L}$ early activation and to Ca^{2+} extrusion from the cell by I_{NaCa}. As apparent in Table 3 the duration of the linear early DD phase is shorter in the KHIS model than in real SAN cells. The recent inclusion in the ML SAN AP model of the phenomenon of spontaneous diastolic local Ca^{2+} release (LCR) has further exhacerbated this aspect, leading to an unbalanced description of DD, with a non-physiological predominance of the non-linear late phase. In our formulation a more realistic balance was achieved in which a linear early DD phase is clearly evident and lasts about 78% of total DD duration as also reported in experiments (Bogdanov *et al.* 2006). It is worth noting that this is fully compatible with the presence of a Ca^{2+}-driven non-linear late DD phase and with the LCR phenomenon, as shown by the presence of a diastolic Ca^{2+} release whose amplitude is modulated by the SERCA pump activity. Our model confirms the ML model prediction that the SERCA pump can modulate pacemaking rate, but within a narrower range than that from their results: grading P_{up} from 1 to 40 mM s^{-1} increased the AP firing rate of our model from 2.7 to 3.9 Hz (Fig. 10*B*), compared to 1.8–4.2 Hz in the ML model. The relevance of I_{NaCa} to late DD and AP upstroke is also confirmed by the stop of pacemaker activity when a substantial I_{NaCa} block was simulated. This result is in line with experiments showing an inhibitory effect of Na^+ replacement by Li^+ on spontaneous beating in SAN cells (Bogdanov *et al.* 2001).

A novel feature of the proposed model is its capability to accurately reproduce the effects of I_f blockade. The most recent SAN models (HSMN and ML) show almost negligible effects of I_f block, although in previous models the increase in cycle length upon block of I_f ranges from 0.9% (Sarai *et al.* (2003)) to 30% (Zhang *et al.* (2000), peripheral cell). Nevertheless all such models, even if useful for theoretical analysis, are now outdated because of lack of species specificity or of detailed description of Ca^{2+} handling, or because they do not take into account more recent experimental data on membrane currents and other mechanisms. Even more importantly, simulations of the effects of I_f block have been often performed in these models by complete abolishment of

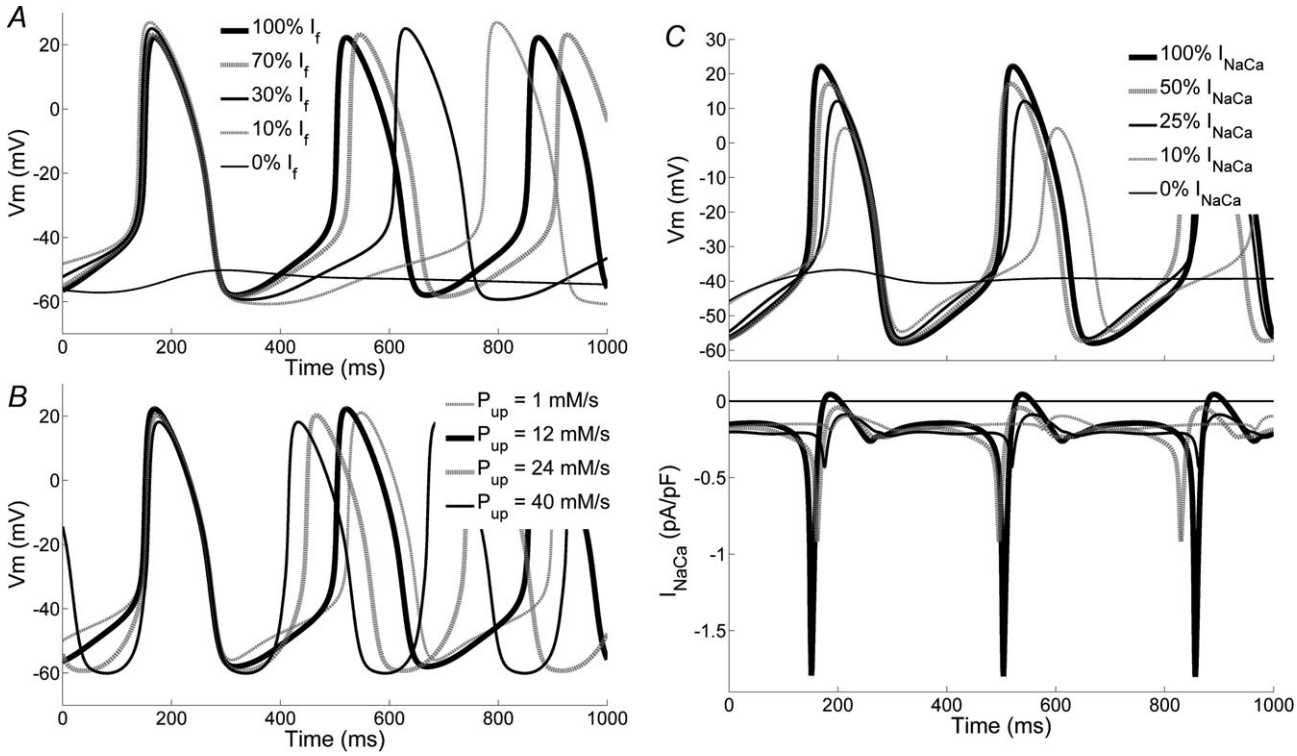

Figure 10. Effects of I_f and I_{NaCa} blockade and Ca^{2+} handling modulation
A, simulation of the effects of increasing level of I_f blockade (0, 30, 70, 90% and 100% conductance reduction) on spontaneous activity. Note that cessation of pacemaking occurs with full I_f block. *B*, effects of changes in Ca^{2+} uptake by SR J_{up} (P_{up} = 1, 12, 24, 40 mM s^{-1}) on simulated activity. *C*, effects of gradual inhibition of Na^+/Ca^{2+} exchange current (100, 50, 25, 10% and 0% residual current) on simulated activity (top); corresponding I_{NaCa} plotted in the bottom panel.

the current. Again, this can be interesting for theoretical analysis, but it turns out not to be correct for validation purposes. In order to validate the computational model, a stringent comparison needs to be made with experimental conditions that have to be reproduced. In particular the specific pharmacological agent used in experiments and its dose–response characteristic has to be considered. This observation, which is obviously valid for any current or mechanism under study, indicates that the weight of I_f has been significantly underestimated in previous models, since the expected amount of I_f block from available experimental data is only partial (see Table 1). Our results demonstrate that it is possible to reproduce realistic I_f rate modulation properties without dramatically change other model components, in particular without modifying the Ca^{2+} handling description. The lack of sensitivity to I_f block in previous models can therefore be a consequence of incorrect estimation of membrane currents during diastolic depolarization, but not only of the I_f current (see results with the Van Ginneken & Giles (1991) kinetics). For example, the sensitivity to I_f block may be 'masked' in previous models by the overestimation of other inward currents such as the sodium background current or the sustained sodium current.

Block of Ca^{2+} transients (in both the cytosol and subsarcolemmal region) in our model reproduces the experimental finding by Himeno *et al.* (2011) that internal BAPTA perfusion, while completely abolishing contractions, maintains rhythmic electrical activity. In our computations the cycle is prolonged during block of Ca^{2+} transients, a result apparent in experimental prolonged perfusion with BAPTA (Himeno *et al.* 2011).

The present model is based on the assumption that the process underlying generation of the early fraction of the DD depends crucially on activation of I_f. The model reproduces the fact that the I_f-dependent early fraction of DD is linear and covers some three-quarters of the entire DD duration (Table 3). The way I_f contributes to determination of pacemaker rate is thus by controlling the slope of early DD. This process is economical, since during early DD the total membrane current is small and a little change in current can alter the steepness substantially, and is efficient, since a small change in steepness results in a substantial alteration of AP rate, obviously under condition of a constant AP threshold.

Contrary to previous SAN models, ours indicates that abolishment of I_f is associated with block of pacemaker

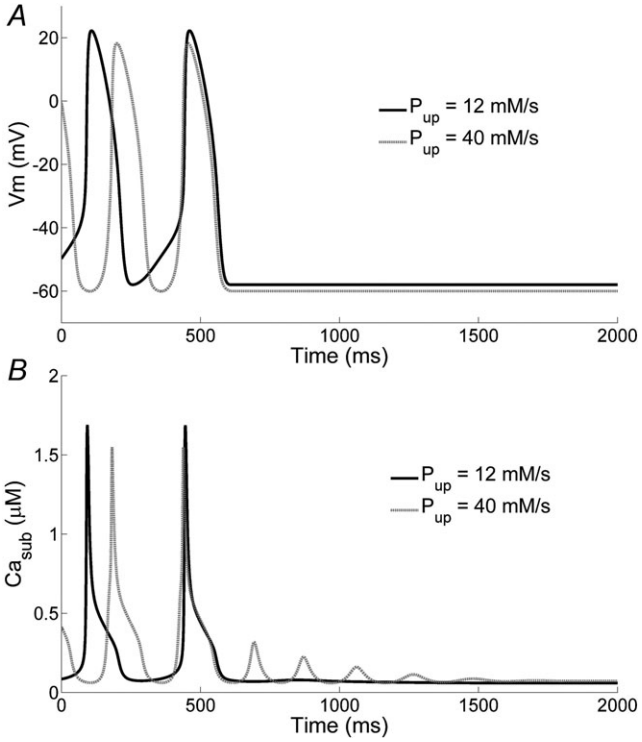

Figure 11. Effects of membrane potential clamp on SR Ca^{2+} release
Simulation of subsarcolemmal Ca^{2+} (Ca_{sub}) concentration dynamics (*B*) when the membrane potential is clamped at MDP (*A*) for $P_{up} = 12$ mM s^{-1} (continuous line) and 40 mM s^{-1} (dashed line). For high values of P_{up} damped Ca^{2+} oscillations are observed.

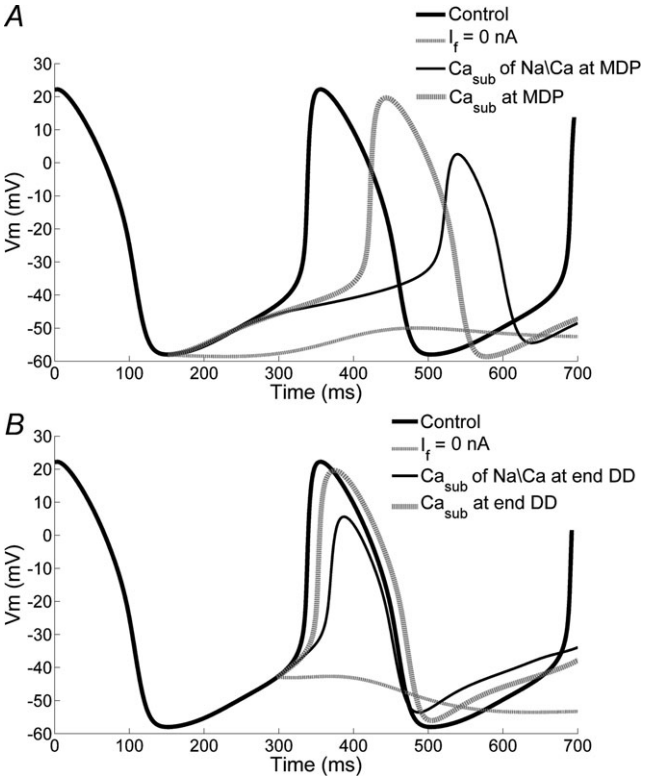

Figure 12. Effects of I_f block or subsarcolemmal Ca^{2+} (Ca_{sub}) clamp during diastolic depolarization (DD)
A, simulations of the effects on membrane potential of I_f block, clamping of Ca_{sub} and clamping of the Ca^{2+} concentration 'sensed' by I_{NaCa} (i.e. the Ca^{2+} term in the I_{NaCa} equations). *B*, the same as in *A*, applied at the beginning of the nonlinear phase of DD.

activity and stabilization of the membrane potential to a resting level of about −50 mV (Fig. 10*A*). To compare this result with *in vitro* data one would need a fully specific f-channel blocker able to block 100% of the current, a condition which, as discussed above, cannot be achieved at present. A better solution to obtain full I_f block is the use of an animal model where conditional, cardiac-specific knockout of HCN4 is performed (Baruscotti *et al.* 2011). Even in this case, the condition of full I_f block is not attained because KO animals die before this occurs; however, the evidence that telemetric *in vivo* rate, spontaneous rate of isolated SAN cells, and I_f conductance decrease in parallel during the KO process (Figs 4 and 5; Baruscotti *et al.* 2011) rules in favour of a strict correlation between the simultaneous presence of I_f and spontaneous activity.

Our computational results do not in any way exclude, and actually support, the idea that changes in the Ca^{2+} transients affect rate. In the late part of DD, a chain of processes takes place which, as in a sort of 'domino effect', makes subsarcolemmal Ca^{2+} elevation activate I_{NaCa} and accelerate depolarization, which effectively 'boosts' the mechanism of $I_{Ca,L}$-triggered AP ignition. This chain of events contributes to determine the total duration of DD, and provides one of the mechanisms participating in the positive chronotropic response to sympathetic stimulation.

The model reproduces the effects of ACh and Iso on rate (Fig. 8). The Iso effect was obtained by shifting the I_f activation curve and modifying other components ($I_{Ca,L}$, I_{Ks} and Na^+/K^+ pump) in accordance with available experimental data; in addition, to mimic sympathetic stimulation the SERCA pump activity was augmented by 25%. This increase is much more modest than that assumed for example in the ML model (100%) based on a parametric analysis aimed to reproduce isoprenaline-induced rate changes, which could not be modified substantially by changes of membrane processes only (Maltsev & Lakatta, 2010). Computational separation of the effects allowed to point out that I_f is the dominant mechanism for Iso induced rate increase in the range up to 30%. It is also worth noting that an Iso-induced increase of the SERCA pump activity larger than that assumed in our simulation can be considered as a functional reserve, still available to reach greater rate increases.

The ACh-induced slowing was obtained by introducing a negative shift of the I_f activation curve and by applying expected changes in $I_{Ca,L}$, $I_{K,ACh}$ and the SERCA pump activity. All the latter changes affected only slightly the rate that was decreased almost entirely because of I_f reduction. As well as reproducing the expected rate changes, our computations show that neither Iso nor ACh modify substantially the TOP, in accordance with experimental data (Bucchi *et al.* 2007).

Limitations

Each numerical model is an imperfect representation of reality, and its limited function is that of verifying the consistency among input data, theoretical assumptions and experimental findings. As with any other model, ours has limitations which restrict its applicability. For example, the Ca^{2+} handling system is likely to be more complex than in our model. We did not include changes due specifically to the activity of the calmodulin kinase II and its dependence upon sympathetic stimulation. However, we used a phenomenological approach and included all Iso-induced changes of elements affecting membrane voltage, thus indirectly integrating also CaMKII-dependent processes.

Clearly, application of this model to a more complete set of experimental conditions will require deeper knowledge and more detailed formulation of these and other mechanisms. Moreover, although the validation using a consistent rabbit SAN-specific data-set strengthens the confidence in the model, it may limit its application in the study of human pathologies.

Conclusion

In conclusion, we developed a novel computational model of physiological cardiac cell pacemaker function able to reproduce a set of recent and less recent experimental data relevant to generation and control of pacemaker activity, and more specifically the changes of pacemaking function associated with changes in I_f current and Ca^{2+} handling as experimentally observed.

References

Altomare C, Terragni B, Brioschi C, Milanesi R, Pagliuca C, Viscomi C, Moroni A, Baruscotti M & DiFrancesco D (2003). Heteromeric HCN1-HCN4 channels: a comparison with native pacemaker channels from the rabbit sinoatrial node. *J Physiol* **549**, 347–359.

Antoons G, Volders PGA, Stankovicova T, Bito V, Stengl M, Vos MA & Sipido KR (2007). Window Ca^{2+} current and its modulation by Ca^{2+} release in hypertrophied cardiac myocytes from dogs with chronic atrioventricular block. *J Physiol* **579**, 147–160.

Barbuti A, Baruscotti M & DiFrancesco D (2007). The pacemaker current: from basics to the clinics. *J Cardiovasc Electrophysiol* **18**, 342–347.

Baruscotti M, Bucchi A, Viscomi C, Mandelli G, Consalez G, Gnecchi-Rusconi T, Montano N, Casali KR, Micheloni S, Barbuti A & DiFrancesco D (2011). Deep bradycardia and heart block caused by inducible cardiac-specific knockout of the pacemaker channel gene Hcn4. *Proc Natl Acad Sci U S A* **108**, 1705–1710.

Bogdanov KY, Maltsev VA, Vinogradova TM, Lyashkov AE, Spurgeon HA, Stern MD & Lakatta EG (2006). Membrane potential fluctuations resulting from submembrane Ca^{2+} releases in rabbit sinoatrial nodal cells impart an exponential phase to the late diastolic depolarization that controls their chronotropic state. *Circ Res* **99**, 979–987.

Bogdanov KY, Vinogradova TM & Lakatta EG (2001). Sinoatrial nodal cell ryanodine receptor and Na^{+}-Ca^{2+} exchanger : molecular partners in pacemaker regulation. *Circ Res* **88**, 1254–1258.

Bois P, Bescond J, Renaudon B & Lenfant J (1996). Mode of action of bradycardic agent, S 16257, on ionic currents of rabbit sinoatrial node cells. *Br J Pharmacol* **118**, 1051–1057.

Bucchi A, Baruscotti M & DiFrancesco D (2002). Current-dependent block of rabbit sino-atrial node I_f channels by ivabradine. *J Gen Physiol* **120**, 1–13.

Bucchi A, Baruscotti M, Robinson RB & DiFrancesco D (2007). Modulation of rate by autonomic agonists in SAN cells involves changes in diastolic depolarization and the pacemaker current. *J Mol Cell Cardiol* **43**, 39–48.

Choi HS, Wang DY, Noble D & Lee CO (1999). Effect of isoprenaline, carbachol, and Cs^{+} on Na^{+} activity and pacemaker potential in rabbit SA node cells. *Am J Physiol Heart Circ Physiol* **276**, H205–H214.

Demir SS, Clark JW, Murphey CR & Giles WR (1994). A mathematical model of a rabbit sinoatrial node cell. *Am J physiol Cell Physiol* **266**, C832–C852.

Denyer JC & Brown HF (1990). Pacemaking in rabbit isolated sino-atrial node cells during Cs^{+} block of the hyperpolarization-activated current if. *J Physiol* **429**, 401–409.

DiFrancesco D (1993). Pacemaker mechanisms in cardiac tissue. *Annu Rev Physiol* **55**, 455–472.

DiFrancesco D (2010). The role of the funny current in pacemaker activity. *Circ Res* **106**, 434–446.

DiFrancesco D, Ducouret P & Robinson RB (1989). Muscarinic modulation of cardiac rate at low acetylcholine concentrations. *Science* **243**, 669–671.

DiFrancesco D, Ferroni A, Mazzanti M & Tromba C (1986). Properties of the hyperpolarizing-activated current (i_f) in cells isolated from the rabbit sino-atrial node. *J Physiol* **377**, 61–88.

DiFrancesco D & Noble D (1982). Implications of the reinterpretation of iK2 for the modelling of the electrical activity of the pacemaker tissues in the heart. In *Cardiac Rate and Rhythm: Physiological, Morphological and Developmental Aspects*, ed. Boumann LN & Jongsma HJ, pp. 93–128. TheHague: Martinus Nijhoff.

DiFrancesco D & Noble D (1985). A model of cardiac electrical activity incorporating ionic pumps and concentration changes. *Philos Trans R Soc Lond B Biol Sci* **307**, 353–398.

DiFrancesco D & Noble D (2012). The funny current has a major pacemaking role in the sinus node. *Heart Rhythm* **9**, 299–301.

DiFrancesco D & Tromba C (1988). Inhibition of the hyperpolarization-activated current (i_f) induced by acetylcholine in rabbit sino-atrial node myocytes. *J Physiol* **405**, 477–491.

Dokos S, Celler B & Lovell N (1996). Vagal control of sinoatrial rhythm: a mathematical model. *J Theor Biol* **182**, 21–44.

Fermini B & Nathan RD (1991). Removal of sialic acid alters both T- and L-type calcium currents in cardiac myocytes. *Am J Physiol Heart Circ Physiol* **260**, H735–H743.

Garny A, Noble D, Hunter PJ & Kohl P (2009). Cellular Open Resource (COR): current status and future directions. *Philos Transact A Math Phys Eng Sci* **367**, 1885–1905.

Hagiwara N, Irisawa H & Kameyama M (1988). Contribution of two types of calcium currents to the pacemaker potentials of rabbit sino-atrial node cells. *J Physiol* **395**, 233–253.

Heath BM & Terrar DA (1996). Separation of the components of the delayed rectifier potassium current using selective blockers of IKr and IKs in guinea-pig isolated ventricular myocytes. *Exp Physiol* **81**, 587–603.

Himeno Y, Sarai N, Matsuoka S & Noma A (2008). Ionic mechanisms underlying the positive chronotropy induced by beta1-adrenergic stimulation in guinea pig sinoatrial node cells: a simulation study. *J Physiol Sci* **58**, 53–65.

Himeno Y, Toyoda F, Satoh H, Amano A, Cha CY, Matsuura H & Noma A (2011). Minor contribution of cytosolic Ca^{2+} transients to the pacemaker rhythm in guinea pig sinoatrial node cells. *Am J Physiol Heart Circ Physiol* **300**, H251–H261.

Honjo H, Boyett MR, Kodama I & Toyama J (1996). Correlation between electrical activity and the size of rabbit sino-atrial node cells. *J Physiol* **496**, 795–808.

Kawano S & Hiraoka M (1991). Transient outward currents and action potential alterations in rabbit ventricular myocytes. *J Mol Cell Cardiol* **23**, 681–693.

Ke Y, Lei M, Collins TP, Rakovic S, Mattick PAD, Yamasaki M, Brodie MS, Terrar DA & Solaro RJ (2007). Regulation of L-Type calcium channel and delayed rectifier potassium channel activity by p21-activated kinase-1 in guinea pig sinoatrial node pacemaker cells. *Circ Res* **100**, 1317–1327.

Kurata Y, Hisatome I, Imanishi S & Shibamoto T (2002). Dynamical description of sinoatrial node pacemaking: improved mathematical model for primary pacemaker cell. *Am J Physiol Heart Circ Physiol* **283**, H2074–H2101.

Lakatta EG & DiFrancesco D (2009). What keeps us ticking: a funny current, a calcium clock, or both? *J Mol Cell Cardiol* **47**, 157–170.

Lakatta EG, Maltsev VA & Vinogradova TM (2010). A coupled SYSTEM of intracellular Ca^{2+} clocks and surface membrane voltage clocks controls the timekeeping mechanism of the heart's pacemaker. *Circ Res* **106**, 659–673.

Lei M & Brown HF (1996). Two components of the delayed rectifier potassium current, IK, in rabbit sino-atrial node cells. *Exp Physiol* **81**, 725–741.

Lei M, Cooper PJ, Camelliti P & Kohl P (2002). Role of the 293b-sensitive, slowly activating delayed rectifier potassium current, iKs, in pacemaker activity of rabbit isolated sino-atrial node cells. *Cardiovasc Res* **53**, 68–79.

Maltsev VA & Lakatta EG (2009). Synergism of coupled subsarcolemmal Ca^{2+} clocks and sarcolemmal voltage clocks confers robust and flexible pacemaker function in a novel pacemaker cell model. *Am J Physiol Heart Circ Physiol* **296**, H594–H615.

Maltsev VA & Lakatta EG (2010). A novel quantitative explanation for the autonomic modulation of cardiac pacemaker cell automaticity via a dynamic system of sarcolemmal and intracellular proteins. *Am J Physiol Heart Circ Physiol* **298**, H2010–H2023.

Maltsev VA & Lakatta EG (2012). The funny current in the context of the coupled-clock pacemaker cell system. *Heart Rhythm* **9**, 302–307.

McAllister RE, Noble D & Tsien RW (1975). Reconstruction of the electrical activity of cardiac Purkinje fibres. *J Physiol* **251**, 1–59.

Nagykaldi Z, Kem D, Lazzara R & Szabo B (1999). Canine ventricular myocyte β_2-adrenoceptors are not functionally coupled to L-type calcium current. *J Cardiovasc Electrophysiol* **10**, 1240–1251.

Nakayama T, Kurachi Y, Noma A & Irisawa H (1984). Action potential and membrane currents of single pacemaker cells of the rabbit heart. *Pflugers Arch* **402**, 248–257.

Nikmaram MR, Boyett MR, Kodama I, Suzuki R & Honjo H (1997). Variation in effects of Cs^+, UL-FS-49, and ZD-7288 within sinoatrial node. *Am j Physiol Heart Circ Physiol* **272**, H2782–H2792.

Nilius B (1986). Possible functional significance of a novel type of cardiac Ca channel. *Biomed Biochim Acta* **45**, K37–K45.

Noble D, DiFrancesco D & Denyer JC (1989). Ionic mechanisms in normal and abnormal cardiac pacemaker activity. In *Neuronal and Cellular Oscillators*, ed. Jacklet JW, pp. 59–85.

Noble D, Noble PJ & Fink M (2010). Competing oscillators in cardiac pacemaking. *Circ Res* **106**, 1791–1797.

Noble D & Noble SJ (1984). A model of sino-atrial node electrical activity based on a modification of the DiFrancesco-Noble (1984) equations. *Proc R Soc Lond B Biol Sci* **222**, 295–304.

Ono K & Ito H (1995). Role of rapidly activating delayed rectifier K^+ current in sinoatrial node pacemaker activity. *Am J Physiol Heart Circ Physiol* **269**, H453–H462.

Quayle JM, Standen NB & Stanfield PR (1988). The voltage-dependent block of ATP-sensitive potassium channels of frog skeletal muscle by caesium and barium ions. *J Physiol* **405**, 677–697.

Rosen MR, Nargeot J & Salama G (2012). The case for the funny current and the calcium clock. *Heart Rhythm* **9**, 616–618.

Renaudon B, Bois P, Bescond J & Lenfant J (1997). Acetylcholine modulates I_f and $I_{K(ACh)}$ via different pathways in rabbit sino-atrial node cells. *J Mol Cell Cardiol* **29**, 969–975.

Sakai R, Hagiwara N, Matsuda N, Kassanuki H & Hosoda S (1996). Sodium–potassium pump current in rabbit sino-atrial node cells. *J Physiol* **490**, 51–62.

Sanguinetti MC & Jurkiewicz NK (1990). Two components of cardiac delayed rectifier K^+ current. Differential sensitivity to block by class III antiarrhythmic agents. *J Gen Physiol* **96**, 195–215.

Sarai N, Matsuoka S, Kuratomi S, Ono K & Noma A (2003). Role of individual ionic current systems in the SA node hypothesized by a model study. *Jpn J Physiol* **53**, 125–134.

Severi S, Corsi C, Rocchetti M & Zaza A (2009). Mechanisms of β-adrenergic modulation of IKs in the guinea-pig ventricle: insights from experimental and model-based analysis. *Biophys J* **96**, 3862–3872.

Shibasaki T (1987). Conductance and kinetics of delayed rectifier potassium channels in nodal cells of the rabbit heart. *J Physiol* **387**, 227–250.

Thollon C, Cambarrat C, Vian J, Prost JF, Peglion JL & Vilaine JP (1994). Electrophysiological effects of S 16257, a novel sino-atrial node modulator, on rabbit and guinea-pig cardiac preparations: comparison with UL-FS 49. *Br J Pharmacol* **112**, 37–42.

van Ginneken AC & Giles W (1991). Voltage clamp measurements of the hyperpolarization-activated inward current I_f in single cells from rabbit sino-atrial node. *J Physiol* **434**, 57–83.

Verkerk AO & Wilders R (2010). Relative importance of funny current in human versus rabbit sinoatrial node. *J Mol Cell Cardiol* **48**, 799–801.

Vinogradova TM, Bogdanov KY & Lakatta EG (2002). β-Adrenergic stimulation modulates ryanodine receptor Ca^{2+} release during diastolic depolarization to accelerate pacemaker activity in rabbit sinoatrial nodal cells. *Circ Res* **90**, 73–79.

Vinogradova TM, Lyashkov AE, Zhu W, Ruknudin AM, Sirenko S, Yang D, Deo S, Barlow M, Johnson S, Caffrey JL, Zhou YY, Xiao RP, Cheng H, Stern MD, Maltsev VA & Lakatta EG (2006). High basal protein kinase a-dependent phosphorylation drives rhythmic internal Ca^{2+} store oscillations and spontaneous beating of cardiac pacemaker cells. *Circ Res* **98**, 505–514.

Wilders R (2007). Computer modelling of the sinoatrial node. *Med Biol Eng Comput* **45**, 189–207.

Wilders R, Hoekstra M, van Ginneken AC & Verkerk AO (2010). β-Adrenergic modulation of heart rate: contribution of the slow delayed rectifier K^+ current (I_{Ks}). *Comput Cardiol* **37**, 629–631.

Wilders R, Jongsma HJ & van Ginneken AC (1991). Pacemaker activity of the rabbit sinoatrial node. A comparison of mathematical models. *Biophys J* **60**, 1202–1216.

Zaza A, Robinson RB & DiFrancesco D (1996). Basal responses of the L-type Ca^{2+} and hyperpolarization-activated currents to autonomic agonists in the rabbit sino-atrial node. *J Physiol* **491**, 347–355.

Zeng J & Rudy Y (1995). Early afterdepolarizations in cardiac myocytes: mechanism and rate dependence. *Biophys J* **68**, 949–964.

Zhang H, Holden AV, Kodama I, Honjo H, Lei M, Varghese T & Boyett MR (2000). Mathematical models of action potentials in the periphery and center of the rabbit sinoatrial node. *Am J Physiol Heart Circ Physiol* **279**, H397–H421.

Author contributions

S.S.: conception and design, data analysis and interpretation, manuscript writing, final approval of manuscript. M.F.: data analysis and interpretation, manuscript writing, final approval of manuscript. L.A.C.: data analysis and interpretation, manuscript writing, final approval of manuscript. D.DiF.: conception and design, data analysis and interpretation, manuscript writing, final approval of manuscript.

Acknowledgements

The authors would like to thank Ivan Cenci and Enrico Ravagli for their contribution in the initial stage of this work. Part of this work was supported by the Ministry of Education, University and Research grant PRIN 2008ETWBTW to DD.